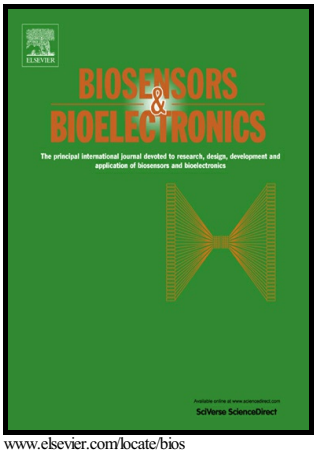

www.elsevier.com/locate/bios

Macroporous Mesh of Nanoporous Gold in Electrochemical Monitoring of Superoxide Release from Skeletal Muscle Cells

Ramin Banan Sadeghian, Jiuhui Han, Serge Ostrovidov, Sahar Salehi, Behzad Bahraminejad, Samad Ahadian, Mingwei Chen, Ali Khademhosseini

PII: S0956-5663(16)30608-X
DOI: http://dx.doi.org/10.1016/j.bios.2016.06.067
Reference: BIOS8859

To appear in: *Biosensors and Bioelectronic*

Received date: 18 May 2016
Revised date: 21 June 2016
Accepted date: 21 June 2016

Cite this article as: Ramin Banan Sadeghian, Jiuhui Han, Serge Ostrovidov Sahar Salehi, Behzad Bahraminejad, Samad Ahadian, Mingwei Chen and Al Khademhosseini, Macroporous Mesh of Nanoporous Gold in Electrochemica Monitoring of Superoxide Release from Skeletal Muscle Cells, *Biosensors an Bioelectronic,* http://dx.doi.org/10.1016/j.bios.2016.06.067

Macroporous Mesh of Nanoporous Gold in Electrochemical Monitoring of Superoxide Release from Skeletal Muscle Cells

Ramin Banan Sadeghian[a,b], *Jiuhui Han*[a], *Serge Ostrovidov*[a], *Sahar Salehi*[a], *Behzad Bahraminejad*[b,c], *Samad Ahadian*[a], *Mingwei Chen*[a], *Ali Khademhosseini*[a,b,d*]

[a]WPI-Advanced Institute for Materials Research, Tohoku University, Sendai 980-8577, Japan

[b]Biomaterials Innovation Research Center, Division of Biomedical Engineering, Department of Medicine, Brigham and Women's Hospital, Harvard Medical School, Boston, MA 02139, USA

[c]Department of Electrical Engineering, Faculty of Engineering, Majlesi Branch, Islamic Azad University, Esfahan 86316-56451, Iran

[d]Harvard-Massachusetts Institute of Technology Division of Health Sciences and Technology, Massachusetts Institute of Technology, Cambridge, MA 02139, USA; Wyss Institute for Biologically Inspired Engineering, Harvard University, Boston, MA 02115, USA; Department of Physics, Faculty of Science, King Abdulaziz University, Jeddah 21569, Saudi Arabia; College of Animal Bioscience and Technology, Department of Bioindustrial Technologies, Konkuk University, Hwayang-dong, Kwangjin-gu, Seoul 143-701, Republic of Korea

[*]Corresponding author: Biomaterials Innovation Research Center, Division of Biomedical Engineering, Department of Medicine, Brigham and Women's Hospital, Harvard Medical School, Boston, MA 02139, USA. Fax: +1 617 768 8477. E-mail address: alik@bwh.harvard.edu (A. Khademhosseini)

Abstract

Real-time monitoring of metabolically relevant biochemicals released in minuscule amounts is of utmost diagnostic importance. Superoxide anion as a primary member of reactive oxygen species, has physiological and pathological effects that depend on its concentration and release rate. Here we present fabrication and successfully testing of a highly sensitive electrochemical biosensor featuring a three-dimensional macroporous mesh of nanoporous gold tailored to measure the dynamics of extracellular superoxide concentration. Wide and accessible surface of the mesh combined with high porosity of the thin nanoporous gold coating enables capturing the analyte in pico- to nano-molar ranges. The mesh is functionalized with cytochrome-*c* (cyt-*c*) and incorporated as a working electrode to measure the release rate of drug-induced superoxide from C2C12 cells through a porous membrane. The device displays a considerably improved superoxide sensitivity of 7.29 nA nM^{-1} cm^{-2} and a low level of detection of 70 pM. Such gain is orders of magnitude higher than any similar enzyme-based electrochemical superoxide sensor and is attributed to the facile diffusion of the analyte through the well-spread nanofeatured gold skin. Superoxide generation rates captured from monolayer myoblast cultures containing about 4×10^4 cells, varied from 1.0 to

9.0 nM min^{-1} in a quasi-linear fashion as a function of drug concentration. This work provides a platform for development of highly sensitive molecular electrochemical biosensors.

Keywords: Noninvasive Electrochemical Biosensor, Hierarchical Nanostructure, Reactive Oxygen Species, Skeletal Muscle Cells, Superoxide Anion Monitoring

1. Introduction

Biosensors are useful in numerous applications in medicine, including biomolecular sensing, monitoring cellular interactions with their microenvironment, and in assessing free radicals such as reactive oxygen and reactive nitrogen species (ROS and RNS) (Calas-Blanchard et al. 2014; Ingebrandt 2015; Qiu et al. 2014; Zhao et al. 2011). Detection of antioxidants, free radicals, and particularly ROS have recently attracted much attention because of their diverse physiological and pathological effects (Halliwell 2006). Such contrasting functions of ROS, and superoxide as the primary member of the group, makes accurate determination of these biospecies an important yet challenging task.

In the context of skeletal muscle tissue, extracellular superoxide rises during contractile activity and fatigue (Kolbeck et al. 1997; Powers and Jackson 2008; Yavari et al. 2015). Such rise is limited within physiologically safe levels and is even known to attenuate during aging (Jackson and McArdle 2011). Superoxide at higher levels, along with other members of ROS, may trigger muscle tissue malfunctioning and damage (Jackson and McArdle 2011; Matecki et al. 2014; Rochard et al. 2000; Sestili et al. 2009).

The longer half-life of superoxide compared to other ROS allows it to move within the cytoplasmic region targeting various organelles. Nonetheless, unlike H_2O_2, it is negatively charged and rather impermeable through the plasma membrane making it difficult to monitor in the extracellular milieu (Murrant and Reid 2001). The uncertainly in the spatiotemporal states of superoxide in the literature accompanied by its concurrent scarceness and volatility

necessitate design of a sensitive, rapid, and noninvasive biosensor capable of targeting and detecting the substance in minuscule amounts and in real-time.

Variety of techniques have been used to detect superoxide in skeletal muscle tissue (Abdel Khalek et al. 2014; Mujahid et al. 2005; Xu et al. 2010), among which the electrochemical methods are favorable because of their inherent sensitivity, fast response times, and nondestructive nature (Flamm 2014; Manning and McNeil 2011; Szilveszter 2011). The physiological concentrations of superoxide are remarkably low, at the nanomolar range, and may shrink even further by undergoing an enzymatic disproportionation reaction with superoxide dismutase (SOD). To be able to monitor the substance at these conditions, even electrochemical biosensors must be placed in a close proximity of the region of interest, making them often impractical for safe *in vivo* operation or to employ at the site of injury (Fujita et al. 2009; Ganesana et al. 2012; Rahman et al. 2012). Ganesana et al. recently employed a gold wire cytochrome-*c* (cyt-*c*) based sensor and measured the accumulation of superoxide in mice brain slices in micro-molar range with a sensitivity of 0.14 nA nM^{-1} cm^{-2} in culture medium (Ganesana et al. 2012). Fujita et al. used a carbon electrode functionalized with a cyt-*c*-mimic synthetic enzyme to measure superoxide concentrations in the right atria of endotoxemin rats (Fujita et al. 2009). They integrated the amperogram over time and expressed the sensor response based on the accumulated charge resulting a sensitivity of 0.41 $\mu C\ \mu M^{-1}$. Recently, Zhu et al. have utilized a porous Pt-Pd construct, decorated with SOD, and detected superoxide in living HeLa cells with a sensitivity of 1.27 nA nM^{-1} (Zhu et al. 2016). Taking into account the importance of ROS levels in physiological and pathological contexts, it is of utmost importance to measure these species in lowest possible amounts, necessitating devices with orders of magnitude higher sensitivities.

Sensors can be technically placed farther provided their sensitivity is enhanced by increasing the electrode surface area. Making a rough surface is one way to achieve this without compromising space. Nanoporous gold (NPG) is a spongy structure comprised of

nanoscale pores and ligaments that offer effective surface areas hundreds to thousands of times larger than bulk gold films of the same volume. Such a large surface area along with the permeable network of nanopores has rendered NPG a desirable construct for the fabrication of sensitive chemical sensors (Collinson 2013; Scanlon et al. 2012).

Recently, we have demonstrated the superior performance of NPG over screen-printed (SP) gold electrodes in superoxide biosensing (Banan-Sadeghian et al. 2016). In this study, the NPG electrode functionalized with cyt-*c* displayed 14 times better sensitivity than the nonporous counterpart, having the same apparent surface area. Although the thick-film NPG offers an electrochemically-active surface area (ESA) a few hundred times wider than the nonporous SP electrode, the sensitivity of the NPG-based electrode toward superoxide does not scale up accordingly. Only a fraction of the electrode volume at the surface is exposed to the surrounding superoxide-containing medium. Nanoscale pores hinder the diffusion of the medium or cyt-*c* well into the bulk of the NPG thick-film. Hence, a large fraction of the electrode remains isolated and unmodified.

Here we present an innovative electrode architecture by wrapping a thin film of mesoporous gold over a metallic cellular matrix, thus resolving the coverage and diffusion issues at the same time and improving the electrode inherent sensitivity. The hierarchical nanofeatured network, referred to as macroporous mesh of nanoporous gold, or simply nanoporous gold mesh (NPGM), was assembled on ultralight nickel foam templates. Ni foams are commercially available, low density, permeable, but mechanically strong metallic platforms with high porosity (75 - 95%). They have a wide range of applications in gas and liquid filters, batteries, vibration-absorbing materials, heat exchangers, optics, etc. (Schaedler et al. 2011; Xia et al. 2015; Xiao et al. 2015) If the macroporous skeleton of the foam is covered by a mesoporous gold layer, the resulting network can offer a tremendously large surface area. In addition, because such layer is thinner and coarser than thick-film NPG, it allows the sensitive enzyme to diffuse and cover a larger fraction of the nanostructure.

Presence of Ni as a cytotoxic element, however, hinders application of the mesh as a noninvasive biosensor. Hence, the entire Ni constituent of NPGM including the core was removed chemically during the dealloying process forming tubular ligaments. The foams were first shielded by a layer of Au to provide mechanical support for the NPG skin once the Ni core is removed. The golden construct was subsequently modified with cyt-*c*. Biosensors built on cyt-*c*-modified NPGM, were interfaced with C2C12 myoblasts through a porous membrane and used to accurately measure the rate of superoxide release in nM min^{-1} upon stimulation. A drastically improved amperometric sensitivity, low limit of detection (LOD), and linear dynamic range over similar superoxide-sensitive enzyme-immobilized electrodes was attained. Such hierarchical nanofeatured construct can provide numerous implications in a broad range of biosensing applications where sensitivity and rapid response matter.

2. Experimental

2.1. Synthesis and characterization of electrodes

NPG films about 1 μm-thick were deposited at the center of screen-printed DropSens strips (DropSens, Spain) as reported earlier (Banan-Sadeghian et al. 2016). NPGM constructs were prepared using commercially available ultralight macroporous Ni foams as templates. The foams (~ 0.04 g cm^{-2} and 1.0 mm in thickness) purchased from Sumitomo Electric Industries, Ltd., were first treated in an HCl solution (1.0 M) for 10 minutes under sonication to remove the native oxide layer and then rinsed with deionized water. Cleaned samples were immersed in an aqueous solution containing $KAu(CN)_2$ (20 mM), ethylenediaminetetraacetic acid tetrasodium salt (EDTA·4Na) (80 mM), triammonium citrate (60 mM), Na_3PO_4 (20 mM) and sodium dodecyl sulfate (0.5 mM, pH = 4) at 50 °C for 12h to substitute the nickel layer at the surface with gold (Yuko et al. 1999). The resulting macroporous Ni/Au (core/shell) sheet was then electroplated with $Au_{18}Ag_{82}$ in a similar fashion to deposition of NPG films, except the electroplating solution was not stirred. Finally, the macroporous Ni/Au/AuAg mesh was

subjected to concentrated HNO_3 (79 wt%) for 12h at room temperature to dealloy the AuAg film and remove the residual Ni. In order to remove the residues of HNO_3, both NPG and NPGM electrodes were thoroughly rinsed with deionized water and stored.

2.2. Miscellaneous experimental procedures

NPG- and NPGM-based electrodes were characterized and then functionalized for superoxide detection. Details of such procedures, along with those of various other experiments (cell culture, electrochemical measurement setup, viability analysis, and signal-to-noise (SNR) calculations) are presented in the supplementary information.

3. Results and discussion

3.1. NPGM Superoxide Electrode; Fabrication and Calibration

The performance of NPGM as a working electrode was evaluated and compared to the earlier reported SP and NPG-covered flat electrode variants. Fig. 1 represents the strategy for the electrochemical detection of superoxide by oxidation at gold electrodes, regardless of the electrode shape and morphology. As illustrated in Fig. 1(a), cyt-*c* is tethered to gold using a SAM of an alkanethiol covalent binder, DTSSP. The disulfide bond acts as an anchor to the Au surface forming an Au-S dative bond, while the activated N-hydroxysulfosuccinimide (Sulfo-NHS) end group grabs the Lysine residues of cyt-*c* (Hermanson 2013). To prevent direct contact with cyt-*c*, C2C12 cell cultures were interfaced with the electrode through a porous polyester membrane (Fig. 1(b)).

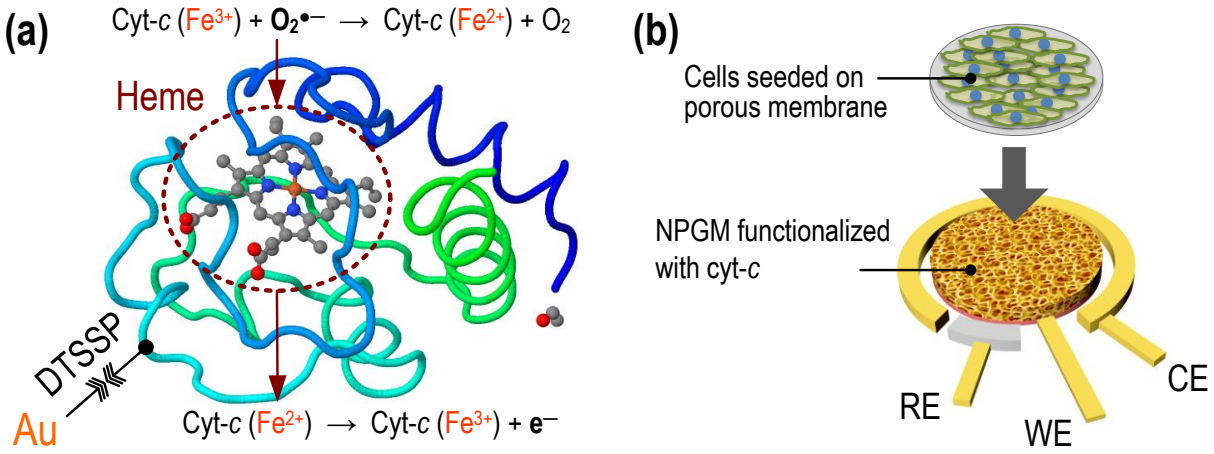

Fig. 1. Electrochemical detection of extracellular superoxide. **(a)** Sensing mechanism by oxidation and direct electron transfer between the redox protein (Cyt-*c*) and the electrode. Fe^{3+} located at the center of the heme group is reduced by an approaching superoxide radical molecule which is in turn reoxidized at the positively biased electrode. **(b)** Cells cultured on a porous membrane are interfaced with the functionalized electrode. WE, CE, and RE denote the working and counter electrodes (Au), and the reference electrode (Ag).

A few micron deep into the crust of the Ni foams, was modified through a displacement reaction that substitutes nickel with gold. The purpose of creating such overlay of gold is to mechanically support the thinner NPG coating once the Ni core is removed for biocompatibility reasons. Samples of the macroporous mesh with gold cladding, were subjected to electrochemical deposition of an $Ag_{82}Au_{18}$ layer that was rendered into NPG through dealloying. The Ni constituent was entirely etched along with Ag during the dealloying process leaving behind a Ni-free tubular golden scaffold with a mesoporous gold sheath. Fig. 2(a,b) show scanning electron microscopy (SEM) images of the final NPGM product focused on a few ligaments and a cross-sectional view of one of the tubular ligaments respectively. The inset in Fig. 2(b) reveals the bilayer configuration of the mesh, where the inner dense Au shell and the outer NPG layer are discernable. Fig. 2(c) illustrates the fabrication process steps schematically.

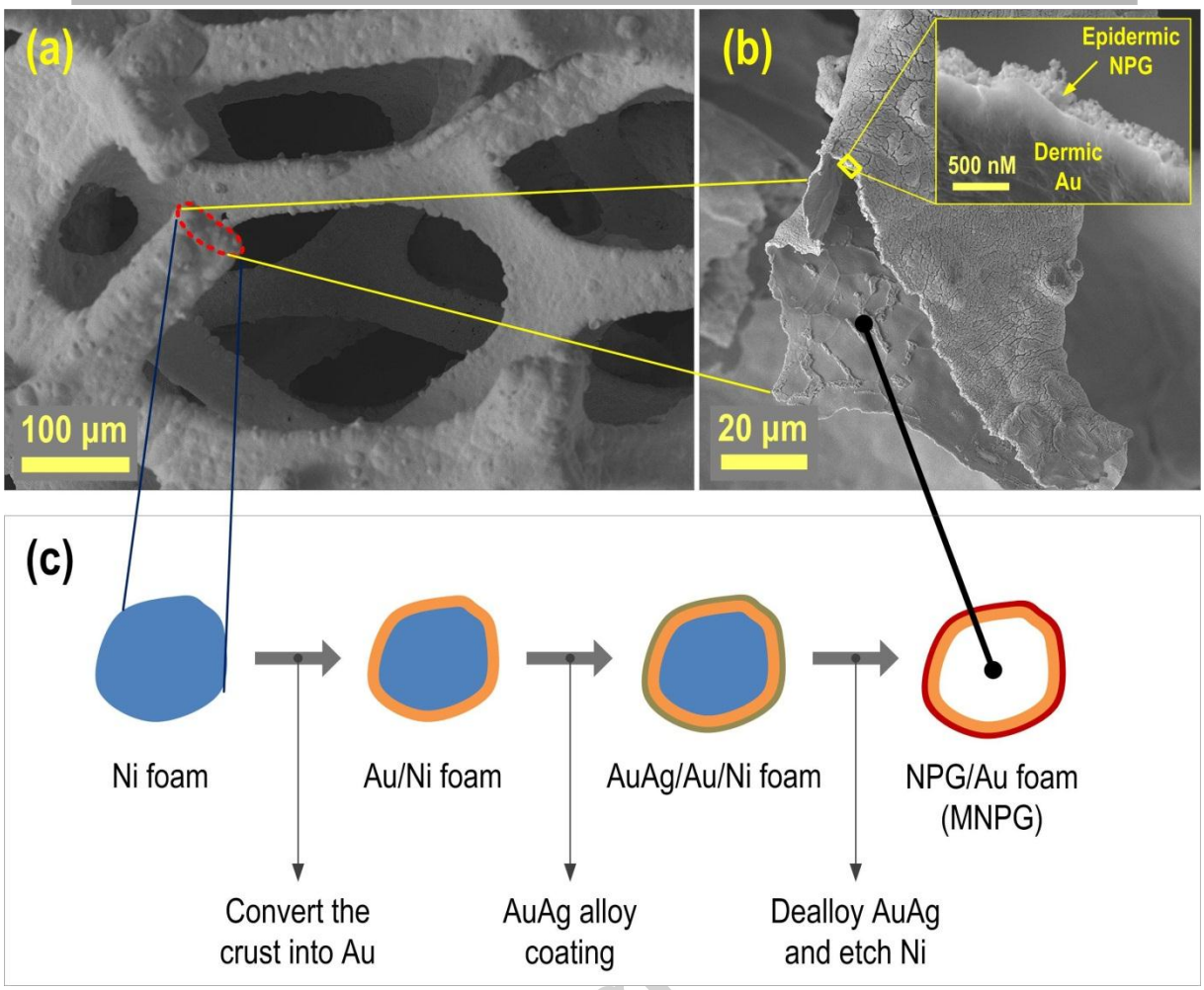

Fig. 2. Fabrication process steps of NPGM. **(a,b)** SEM micrographs showing the bilayer structure of the tubular ligaments. **(c)** Schematic view of the cross-section of a ligament showing the fabrication steps leading to the final NPGM construct.

Fig. 3(a-c) show the physical appearance of the SP and NPG-covered flat electrode surfaces and the NPGM. ESAs were estimated from the voltammograms (Fig. 3(d,e)) and presented in Fig. 3(f). Noticeably, the flat NPG film retains the largest ESA, or equivalently the roughest surface, with NPGM coming second. This is indeed because the NPG film deposited onto the flat SP electrode is noticeably thicker than the same mesoporous layer formed on the macroporous mesh. Although the electrodeposition and dealloying methods were similar for both platforms, the Au/Ag electroplating solution was magnetically stirred in the former, causing a substantially higher deposition rate. As Ni is highly cytotoxic (Kane et al. 2009), it is imperative that no trace of Ni subsequently remain on the NPGM electrodes.

The energy-dispersive x-ray spectroscopy (EDS) spectrum of the macroporous mesh captured after the Ni-to-Au displacement reaction and the spectrum recorded after the deposition of NPG followed by Ni removal are shown in Fig. 3(g). It is clear that the peaks associated to Ni are disappeared in the final NPGM product, making it a suitable and biologically safe substrate to interface with living cells.

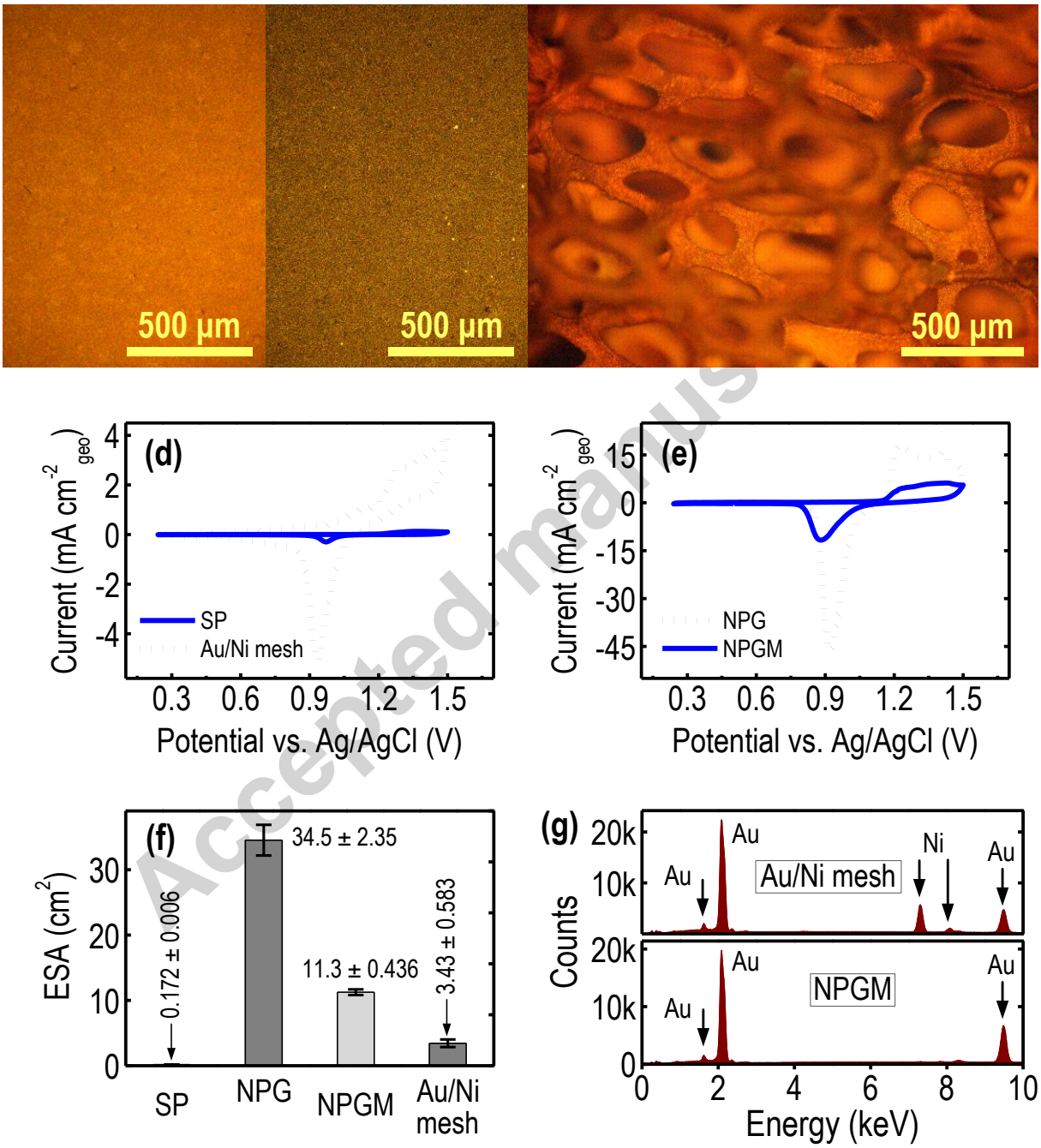

Fig. 3. Electrode surface appearance and characteristics. **(a-c)** Optical microscopy images taken from the surface. **(d,e)** Cyclic voltammograms captured for the purpose of ESA calculations. **(f)** ESA values. The ESA of the Ni mesh after shielding with Au (Au/Ni mesh) is given for comparison reasons. No sensors were built on such structure. Error bars represent

standard deviation (n = 3). **(g)** EDS data showing the surface composition of the macroporous mesh after Au displacement reaction (top) and after NPG deposition followed by Ni removal (bottom). Traces of Ni, still discernable after the displacement process, are completely vanished in the final product.

The surface morphology of three different gold structures incorporated as the electrodes are displayed in the SEM micrographs of Fig. 4(a-c). The TEM and SEM snapshots at the insets of Fig. 4(b) and Fig. 4(c) show nanoscale textures of the NPG film deposited on a SP electrode, and the NPG film deposited on the gold mesh respectively. Pore sizes are independent from the film thickness, though closely related to the dealloying conditions. The prolonged, for up to 12h, and harsh dealloying process in concentrated nitric acid amplifies surface-diffusion of gold atoms (Ding et al. 2004; Erlebacher et al. 2001). This subsequently gives rise to the coarser porous structure of the NPG layer deposited on the macroporous mesh. Such dealloying condition was chosen to simultaneously remove Ag and Ni.

Before use, all biosensors were individually subjected to xanthine/xanthine oxidase (XOD) enzymatic reaction for calibration. At steady-state the net concentration of superoxide, [SO], becomes proportional to the square root of enzyme activity, $[XOD]^{1/2}$ (Tammeveski et al. 1998). Fig. 4(d) shows the calibration curves extracted from amperograms recorded from a sample sensor of each type. Sample calibration amperograms are shown in Fig. S2. The devices were operated in saturated xanthine solution while aliquots of XOD containing known amounts of the enzyme were added sequentially. The amplitude of the currents after attaining steady-state were plotted against the corresponding [SO] value. Sensor gain or sensitivity, S, is defined as the slope of the aforementioned curves and is expressed in nA nM^{-1}, or in nA nM^{-1} cm^{-2} if normalized to the electrode apparent surface area. Note that the apparent surface area of the NPGM electrode corresponds to the ESA of the Ni mesh after coating with the dense Au layer (before NPG was deposited).

Although the NPG-covered electrode exhibits a larger ESA (Fig. 3(f)), the entire volume of the porous film is not coated by cyt-*c* nor exposed to the ambient medium. As illustrated schematically in Fig. 4(e), diffusion is limited to a shallow layer at the surface of the NPG-coated electrode due to its dense porous structure. Such a superficial coverage also blocks rest of the network, reducing its exposure to the analyte to be sensed. Presence of voids in the NPGM network however, facilitate a better coverage although the NPG sheath is thinner. As a result, a markedly higher sensitivity is furnished. Fig. S3(a-c) display a sample amperogram recorded by an NPGM-based biosensor that is processed through wavelet denoising for the purpose of SNR calculation. Table I summarizes gain data statistics of sensors employing three different types of gold electrodes whether functionalized with cyt-*c* or without any coating (bare gold). As expected, regardless of electrode morphology, cyt-*c*-immobilized gold electrodes exhibited a higher sensitivity than those of bare gold (see supplementary information). The NPGM based device stands out for its exceptional gain and SNR. In addition, the specificity of the superoxide biosensor was confirmed by using SOD as a superoxide scavenger (Fig. S4).

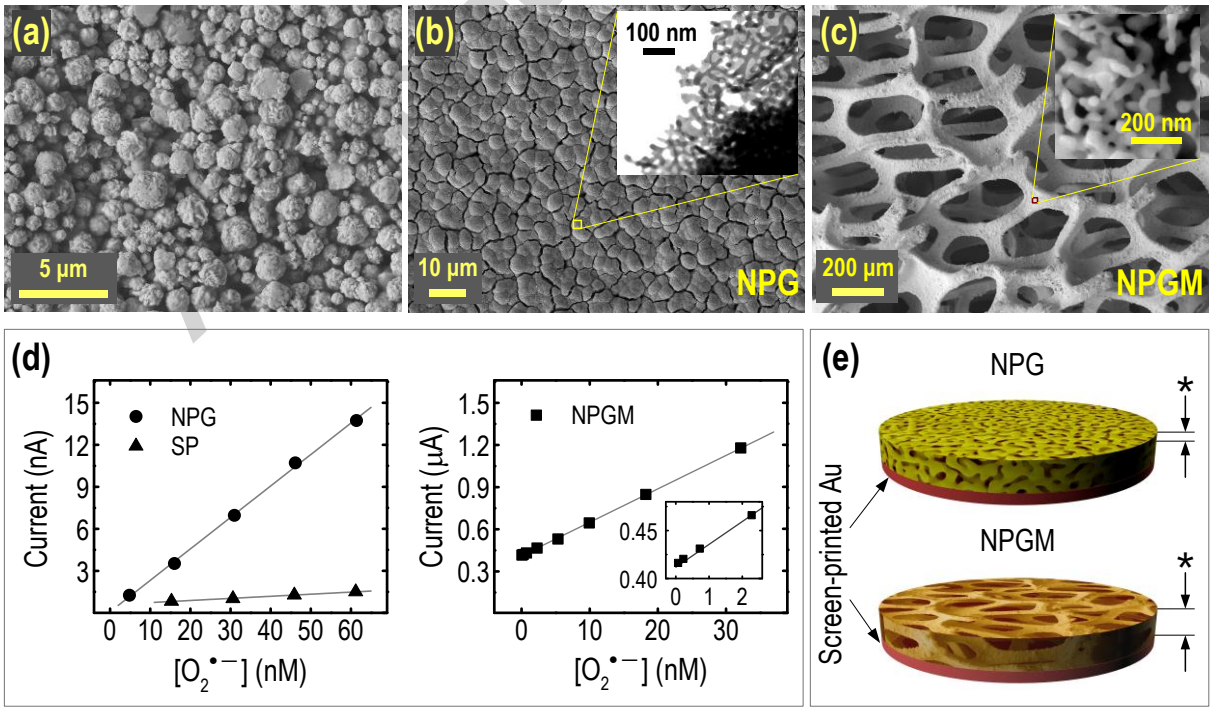

Fig. 4. Electrode surface morphology and superoxide sensitivity. SEM micrographs taken from the surface of **(a)** SP, (**b)** NPG-covered, and **(c)** NPGM electrode samples. The snapshots at the inset of **(b)** and **(c)** show the corresponding surface nanostructures. **(d)** Calibration curves of representative sensors were obtained by running the devices in xanthine/XOD system. The curve in the inset shows performance of the NPGM electrode at low superoxide concentrations (μA vs nM). **(e)** Schematic illustrations of the NPG-covered and NPGM electrodes signifying limited diffusion and coverage of cyt-*c* and the medium in the former (*).

The low limit of detection (LOD) for the sensors is defined as the smallest superoxide concentration the devices can reliably detect. Estimated LODs were 4.84 nM and 70 pM for the NPG and NPGM based biosensors respectively. These values however, correspond to superoxide concentrations generated by the lowest possible dose of XOD that could be added to the saturated xanthine background (0.3 mU L^{-1}). Hence, the actual figures may even be smaller. A comparison among the specifications of various reported superoxide electrochemical biosensors is presented in Table S-I. All of these devices are functionalized with superoxide-sensitive enzymes, cyt-*c* or SOD, and operate based on the same principle. We believe only the work of Rahman et al. has a comparable performance to that of the present work (Rahman et al. 2012). They argued that the activity of cyt-*c* immobilized through SAMs of organic molecules decreases in the absence of a biological support. Instead, they coimmobilized cyt-*c* with a lipid onto a conductive polymer (CP) deposited on a gold microelectrode (Au/CP/lipid/cyt-*c*). The high inherent sensitivity of the microelectrode was attributed to the increased electron transfer rate of the redox protein at the CP, as well as the suitable medium lipid provides for the immobilization of cyt-*c*. Nevertheless, their Au microelectrode was operated in direct contact with rat brain tissue to detect extracellular release of the analyte. We foresee if such lipid-embedded compound is applied on the massively porous NPGM, in lieu of direct covalently bonded cyt-*c*, even a higher sensitivity can be achieved.

Table 1. Superoxide biosensor geometrical specifications and gain statistics

Electrode type	Surface area [cm^2]		Gain [nA nM^{-1}]			
	Apparent	ESA	cyt-*c*	bare Au	SNR (dB)	LOD [nM]
SP	0.126	0.172 ± 0.006	0.017 ± 0.003	N/A	12.2	N/A
NPG-covered	0.126	34.525 ± 2.349	0.240 ± 0.062	0.049 ± 0.001	20.5	4.84
NPGM	3.43 ± 0.583[a]	11.249 ± 0.436	**25.0 ± 11.3**	**5.25 ± 0.986**	**33.2**	**0.07**

[a] The apparent surface area of the NPGM structure is equivalent to its ESA prior to deposition of NPG. Errors (±) are given in form of standard deviation of the measured quantities.

3.2. Application of NPGM as a Biosensor, Measuring the Rate of Superoxide Released from Skeletal Muscle Cells

Porous polyester membranes carrying C2C12 myoblasts in confluency, after two days of culture, were mounted on cyt-*c*-functionalized electrodes and then immediately transferred to an electrochemical cell where stimulus and measurements were performed. Sample amperograms captured by the NPGM-based biosensor corresponding to different stimulus concentrations, [PMA], are shown in Fig. S5(a-c). The new device, displayed a significantly amplified response, about two orders of magnitude higher than that of earlier NPG-based sensor (Banan-Sadeghian et al. 2016). Extracellular superoxide would have needed to diffuse through the pores of 10 μM-thick polyester membranes, with a high chance of recombination, before reaching the surface of cyt-*c* coated electrodes. Consequently, in the context of skeletal muscle tissue, it is not only clinically relevant but also more reasonable and precise here to quantify the rate of generation, $[SO]^{\bullet}$, instead of the absolute concentration of superoxide ([SO]). As illustrated in the sample amperogram of Fig. S5(d), these rates were obtained from the slope of the current response using

$$[SO]^{\bullet} = dI/dt \cdot S^{-1}, \quad (1)$$

where *dI/dt* is the slope of the linear regression fit to the amperogram after the current begins to ramp.

The graph in Fig. 5a shows the recorded $[SO]^{\bullet}$ values as a function of [PMA]. A fresh sensor/membrane set was used for each test and at least five attempts were made to obtain each datum. Within the studied range, the rates increased with drug concentration in a semi-linear fashion. The degree of such increase was estimated from the slope of the curve as $d[SO]^{\bullet} / d[PMA] = 1$ nM min^{-1} per μM of PMA. The minimum reproducible rate was in the order of 1 nM min^{-1} produced by 0.65μM of PMA. Lower dosages of the drug failed to generate any consistent measurable superoxide signal. Remarkably, these rates (1.1 to 8.9 nM min^{-1}) are not only within the range of physiologically generated superoxide rates, reported previously on contractile skeletal muscle bundles, but also match our earlier electrochemical measurements (Banan-Sadeghian et al. 2016; Kobzik et al. 1994; Kolbeck et al. 1997).

To study and quantify possible adverse effects PMA can cause on the dynamics, repeatability, and rate of superoxide bursts, subsequent doses of the same drug were administered sequentially, once the response to the previous stimulus had settled. Fig. 5b shows the graph of superoxide rates captured when the drug was added sequentially in ~1000 second intervals. Fig. S6 shows a sample amperogram recorded during such sequential stimulation. We noticed that when PMA aliquots were added in cascade to the same sample, the degree of superoxide-generation rate upsurge with drug concentration slows down to 40% of the respective value obtained when the rates were recorded by adding PMA to fresh cells. Finally, it is worth to emphasize that upon administration of PMA, current ramped with a rate that was consistently scaled with the drug concentration, allowing us to compute $[SO]^{\bullet}$. In addition, live/dead staining experiments indicated that cell viability was not affected during our experiments (Fig. S7).

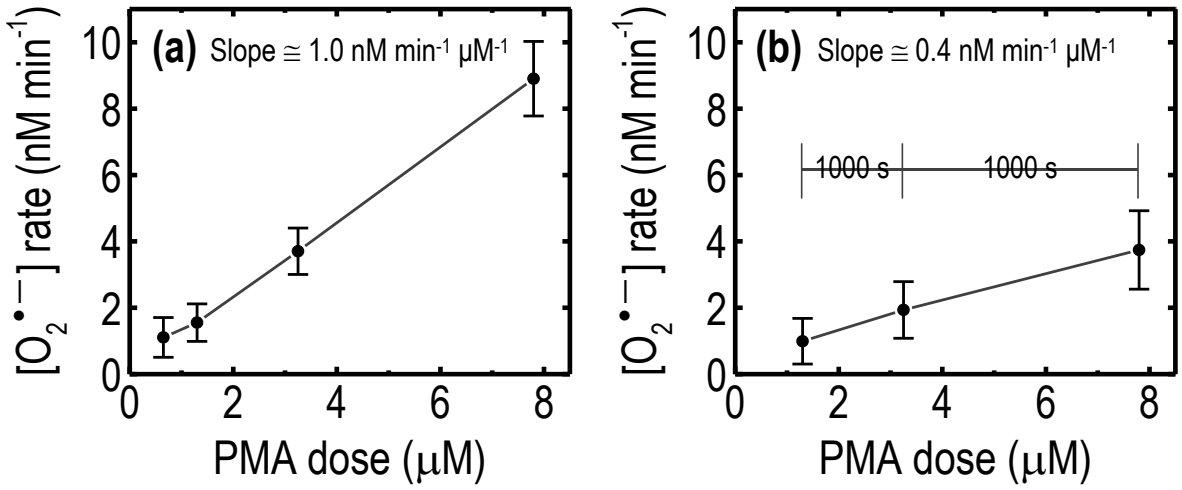

Fig. 5. Superoxide generation rates of C2C12 myoblasts plotted as a function of PMA concentration. **(a)** PMA added to fresh cells/sensors. (**b)** PMA added sequentially in 1000 second intervals. Rates were not normalized to the number of cell nuclei. Error bars represent standard deviation (n = 5).

4. Conclusion

A hierarchical three-dimensional network of mesoporous Au with a markedly rough and wide surface, was modified with cyt-*c* and employed to target superoxide anions released from skeletal muscle tissue. The device exhibited a considerably amplified response to drug induced oxidative burst. Namely, the sensitivity of the biosensor was improved two to three orders of magnitude over the earlier reported devices. Other groups have detected superoxide levels from immortal cell lines, glioblastoma, etc. using a similar strategy. However, in view of the importance of superoxide dynamics in vital organs, such as heart and skeletal system, our NPGM based sensor offers a unique advantage in online monitoring of the analyte in muscle and muscle-like tissues. Ongoing research is focused on measuring the rate of superoxide release from C2C12 cell line subjected to electrical stimulation.

Appendix A. Supporting material

Supplementary data associated with this article can be found in the online version at http://

Acknowledgements

We would like to thank Prof. Susumu Ikeda for providing the Keithley 4200 semiconductor parameter analyzer, and Mr. Amir Nasajpour for his insights on the chemistry of SAMs and cell adhesion mechanisms. We also appreciate the financial support of KAKENHI Grants-in-Aid program (Grant Number 15K16318).

Serge Ostrovidov and Sahar Salehi contributed equally to this work.

A macroporous mesh of nanoporous gold is fabricated on a Ni-based scaffold. After removal of the Ni template, the hierarchical nanofeatured construct is utilized as a working electrode of an electrochemical biosensor tailored to measure the concentration of ambient superoxide. Once interfaced with C2C12 cells, the device measures the rate of extracellular superoxide generation in nanomolar per minute upon stimulation.

Noninvasive Electrochemical Biosensor, Hierarchical Nanostructure, Reactive Oxygen Species, Skeletal Muscle Cells, Superoxide Anion Monitoring

R. Banan Sadeghian, J. Han, S. Ostrovidov, S. Salehi, B. Bahraminejad, Samad Ahadian, M. Chen, A. Khademhosseini*

Macroporous Mesh of Nanoporous Gold in Electrochemical Monitoring of Superoxide Release from Skeletal Muscle Cells

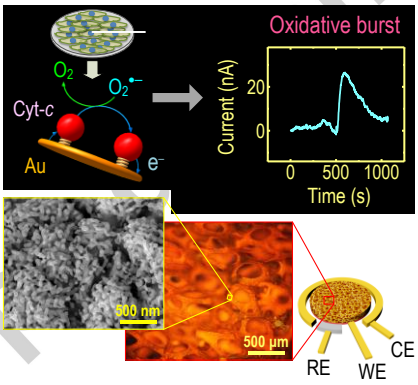

References

Abdel Khalek, W., Cortade, F., Ollendorff, V., Lapasset, L., Tintignac, L., Chabi, B., Wrutniak-Cabello, C., 2014. PLoS One 9(12), e114388.
Banan-Sadeghian, R., Ostrovidov, S., Han, J., Salehi, S., Bahraminejad, B., Bae, H., Chen, M., Khademhosseini, A., 2016. ACS Sensors, *in press*.
Calas-Blanchard, C., Catanante, G., Noguer, T., 2014. Electroanal. 26(6), 1277-1286.
Collinson, M.M., 2013. ISRN Anal. Chem. 2013, 21.
Ding, Y., Kim, Y.J., Erlebacher, J., 2004. Adv. Mater. 16(21), 1897-1900.

Erlebacher, J., Aziz, M.J., Karma, A., Dimitrov, N., Sieradzki, K., 2001. Nature 410(6827), 450-453.
Flamm, H., 2014. Electrochemical Microsensors for Superoxide Monitoring in Cell Culture [Ph.D thesis]. Institut für Mikrosystemtechnik (IMTEK), Lehrstuhl für Sensoren. University of Freiburg, Freiburg, Germany.
Fujita, M., Tsuruta, R., Kasaoka, S., Fujimoto, K., Tanaka, R., Oda, Y., Nanba, M., Igarashi, M., Yuasa, M., Yoshikawa, T., Maekawa, T., 2009. Free. Radic. Biol. Med. 47(7), 1039-1048.
Ganesana, M., Erlichman, J.S., Andreescu, S., 2012. Free. Radic. Biol. Med. 53(12), 2240-2249.
Halliwell, B., 2006. Plant Physiol. 141(2), 312-322.
Hermanson, G.T., 2013. Chapter 3 - The Reactions of Bioconjugation. In: Hermanson, G.T. (Ed.), Bioconjugate Techniques (Third edition), pp. 229-258. Academic Press, Boston.
Ingebrandt, S., 2015. Nat. Nano. 10(9), 734-735.
Jackson, M.J., McArdle, A., 2011. J. Physiol. 589(9), 2139-2145.
Kane, M.A., Kasper, C.E., Kalinich, J.F., 2009. Toxicol. In Vitro 23(2), 356-359.
Kobzik, L., Reid, M.B., Bredt, D.S., Stamler, J.S., 1994. Nature 372(6506), 546-548.
Kolbeck, R., She, Z.-W., Callahan, L., Nosek, A., 1997. Am. J. Respir. Crit. Care Med. 156(1), 140-145.
Manning, P., McNeil, C.J., 2011. Biochem. Soc. Trans. 39(5), 1288-1292.
Matecki, S., Fauconnier, J., Lacampagne, A., 2014. Reactive Oxygen Species and Muscular Dystrophy. In: Laher, I. (Ed.), Systems Biology of Free Radicals and Antioxidants, pp. 3055-3079. Springer Berlin Heidelberg.
Mujahid, A., Yoshiki, Y., Akiba, Y., Toyomizu, M., 2005. Poult. Sci. 84(2), 307-314.
Murrant, C.L., Reid, M.B., 2001. Microsc. Res. Tech. 55(4), 236-248.
Powers, S.K., Jackson, M.J., 2008. Physiol. Rev. 88(4), 1243-1276.
Qiu, L., Zhang, T., Jiang, J., Wu, C., Zhu, G., You, M., Chen, X., Zhang, L., Cui, C., Yu, R., Tan, W., 2014. J. Am. Chem. Soc. 136(38), 13090-13093.
Rahman, M.A., Kothalam, A., Choe, E.S., Won, M.-S., Shim, Y.-B., 2012. Anal. Chem. 84(15), 6654-6660.
Rochard, P., Rodier, A., Casas, F., Cassar-Malek, I., Marchal-Victorion, S., Daury, L., Wrutniak, C., Cabello, G., 2000. J. Biol. Chem. 275(4), 2733-2744.
Scanlon, M.D., Salaj-Kosla, U., Belochapkine, S., MacAodha, D., Leech, D., Ding, Y., Magner, E., 2012. Langmuir 28(4), 2251-2261.
Schaedler, T.A., Jacobsen, A.J., Torrents, A., Sorensen, A.E., Lian, J., Greer, J.R., Valdevit, L., Carter, W.B., 2011. Science 334(6058), 962-965.
Sestili, P., Barbieri, E., Martinelli, C., Battistelli, M., Guescini, M., Vallorani, L., Casadei, L., D'Emilio, A., Falcieri, E., Piccoli, G., Agostini, D., Annibalini, G., Paolillo, M., Gioacchini, A.M., Stocchi, V., 2009. Mol. Nutr. Food Res. 53(9), 1187-1204.
Szilveszter, G., 2011. Detection of Superoxide and Hydrogen Peroxide from Living Cells Using Electrochemical Sensors. Oxidative Stress: Diagnostics, Prevention, and Therapy, pp. 289-309. American Chemical Society.
Tammeveski, K., Tenno, T.T., Mashirin, A.A., Hillhouse, E.W., Manning, P., McNeil, C.J., 1998. Free Radic. Biol. Med. 25(8), 973-978.
Xia, Y., Zhu, D., Si, S., Li, D., Wu, S., 2015. J. Power Sources 283, 125-131.
Xiao, L., Song, W., Tang, H., Zhu, Z., Wang, J., Wang, H., 2015. Mater. Des. 85, 47-53.
Xu, X., Thompson, L.V., Navratil, M., Arriaga, E.A., 2010. Anal. Chem. 82(11), 4570-4576.
Yavari, A., Javadi, M., Mirmiran, P., Bahadoran, Z., 2015. Asian. J. Sports. Med. 6(1), e24898.
Yuko, T., Setsuo, A., Inoue, T., Toshimitsu, N., 1999. Electroless gold plating solution and gold plating method. In: Hitachi Ltd., Japan patent 11-21672.

Zhao, W., Schafer, S., Choi, J., Yamanaka, Y.J., Lombardi, M.L., Bose, S., Carlson, A.L., Phillips, J.A., Teo, W., Droujinine, I.A., Cui, C.H., Jain, R.K., Lammerding, J., Love, J.C., Lin, C.P., Sarkar, D., Karnik, R., Karp, J.M., 2011. Nat. Nano. 6(8), 524-531.
Zhu, X., Liu, T., Zhao, H., Shi, L., Li, X., Lan, M., 2016. Biosens. Bioelectron. 79, 449-456.